48th AIAA Aerospace Sciences Meeting Including the New Horizons Forum and Aerospace Exposition
4 - 7 January 2010, Orlando, Florida
AIAA 2010-1061

Hypersonic Boundary-Layer Transition Experiments in a Mach-6 Quiet Tunnel

Dennis C. Berridge*, Amanda Chou*, Christopher A.C. Ward*,
Laura E. Steen*, Peter L. Gilbert*, Thomas J. Juliano*, and Steven P. Schneider†
School of Aeronautics and Astronautics, Purdue University, West Lafayette, IN 47907-1282

Joel E. Gronvall*
Department of Aerospace Engineering and Mechanics, University of Minnesota, Minneapolis, MN 55455

The Boeing/AFOSR Mach-6 Quiet Tunnel has achieved quiet flow to stagnation pressures of 146 psia, and intermittently quiet flow between 146 and 169 psia. In an attempt to measure natural transition under quiet flow, a 3-m-circular-arc compression cone was tested with a nearly sharp nosetip. Using temperature-sensitive paint, hot streaks were observed to develop near the rear of the cone at high pressures under quiet flow. The streaks do not appear under noisy flow. The cause of the hot streaks remains unknown, though they may be instabilities or artifacts of nonlinear breakdown. Under quiet flow, the cone boundary layer remained laminar up to N factors of at least 15 and possibly as high as 19. Transition occurred at $N = 9$ under noisy flow. It is unknown why laminar flow persisted to such high N factors. As part of an investigation of crossflow vortices, a 7° half-angle cone was tested at 6° angle of attack with temperature-sensitive paint finishes of varying roughness. The roughness of the paint finish was observed to have an effect on crossflow vortices, in some cases inducing transition under noisy flow. Heat-transfer measurements were made at the stagnation point of a hemisphere to observe the effect of freestream noise; no effect was evident.

Nomenclature

A	disturbance amplitude
A_0	initial disturbance amplitude
D	diameter
f	frequency (kHz)
H	enthalpy
M	Mach number
N	integrated amplification factor
p	pressure (psia)
q	dynamic pressure
Re	Reynolds number
St	Stanton number
T	temperature (°C or K)
t	time (seconds)
U	velocity
x	cone axial coordinate (m or cm)
y	cone spanwise coordinate (m or cm)
ρ	density
μ	dynamic viscosity

Superscript	
$'$	fluctuations
Subscript	
0	stagnation condition
∞	freestream condition
i	initial condition
mean	average (mean)
s	model surface
w	wall condition
θ	momentum thickness
2	condition behind shock

Abbreviations	
BAM6QT	Boeing/AFOSR Mach 6 Quiet Tunnel
CEV	Crew Exploration Vehicle
LST	Linear Stability Theory
PSD	Power Spectral Density

*Research Assistant, Student Member AIAA
†Professor, Associate Fellow AIAA

Abbreviations, cont.

PSE	Parabolized Stability Equations
RMS	Root Mean Square
SB	Schmidt-Boelter
TSP	Temperature Sensitive Paint

I. Introduction

Hypersonic laminar-turbulent transition is important for predictions of heat transfer, skin friction, separation, and other boundary-layer properties. However, the transition process is poorly understood, making predictions of transition location uncertain. Vehicles that spend significant portions of their flight at hypersonic speeds can be critically affected by the uncertainties in transition location. Reducing these uncertainties requires better understanding of the transition process, in order to develop more accurate prediction methods.

Simple empirical correlations based on parameters such as Re_θ/M_e (momentum-thickness Reynolds number divided by edge Mach number) are commonly used to estimate transition location. However, their empirical nature makes it difficult to extend results from one vehicle or condition to a highly different flow. Linear Stability Theory (LST) and the Parabolized Stability Equations (PSE) can be used to predict the growth of the boundary layer instabilities which lead to transition. Used with the semi-empirical e^N method, predictions of transition location can be obtained that agree better with experimental data than those found using more empirical methods.[1] The e^N method uses LST or PSE to compute the integrated growth of the instabilities for a given geometry and set of flow conditions, though without knowledge of their initial amplitude. The growth is expressed as $A/A_0 = e^N$, where A is the current amplitude of the instability, and A_0 is the initial amplitude before amplification takes place. Transition location can then be empirically correlated to a certain value of N. This method allows some modeling of the mechanisms which cause transition, giving better accuracy across a wider range of conditions than purely empirical methods.

There have been many transition experiments in ground test facilities over the last 50 years.[2] One way in which the environment in most facilities differs from flight is the high level of freestream disturbances which are radiated from the turbulent boundary layers that are typically present on wind tunnel walls.[3] These disturbance (or noise) levels are typically an order of magnitude larger than those observed in flight.[4,5] Higher noise levels can cause transition to occur much earlier than is observed in flight.[3,5] Transition typically corresponds well to N factors of about 5 in conventional facilities,[1] whereas in low-noise (quiet) facilities, as well as in flight, N factors at the location of transition are usually between 8 and 11.[5,6] Quiet facilities are important to understanding the relationship between transition experiments in conventional tunnel facilities and transition in flight. Quiet facilities are typically restricted to lower Reynolds numbers, where it is easier to maintain a laminar boundary layer on the nozzle wall.[7] This restriction makes it difficult to observe transition on most models, since the instabilities do not become large enough to break down to turbulence without being induced artificially, i.e. using roughness elements or a controlled disturbance.

II. The Boeing/AFOSR Mach-6 Quiet Tunnel

The Boeing/AFOSR Mach-6 Quiet Tunnel (BAM6QT) is presently the only operational hypersonic quiet tunnel in the world. The tunnel was designed as a Ludwieg tube in order to minimize complexity and the cost of building and operating the facility. The tunnel configuration is shown in Figure 1. The BAM6QT is designed for a maximum stagnation pressure of 300 psia (2 MPa) and a maximum quiet pressure of 150 psia (1 MPa). The noise level (root-mean-square of the pitot pressure fluctuations normalized by the stagnation pressure) of the tunnel under quiet flow is less than 0.05%, and under noisy flow is about 3%. The BAM6QT uses many design features to delay transition in the nozzle-wall boundary layer, maintaining a laminar boundary layer and thus low noise levels. These features include a suction slot upstream of the throat, which removes the boundary layer that has developed on the contraction. Removing the boundary layer through the slot allows a fresh, laminar boundary layer to grow on the expanding portion of the nozzle. This suction slot is connected to the vacuum tank (Figure 1) through a valve that can be opened for quiet operation or closed for operation with noise levels comparable to a conventional facility. Among the other features are a long nozzle designed to reduce the growth of Görtler vortices, a highly polished throat, and high-quality air filters to ensure a clean-room environment inside the tunnel. A more thorough description of the design and components of the BAM6QT can be found in Reference 7.

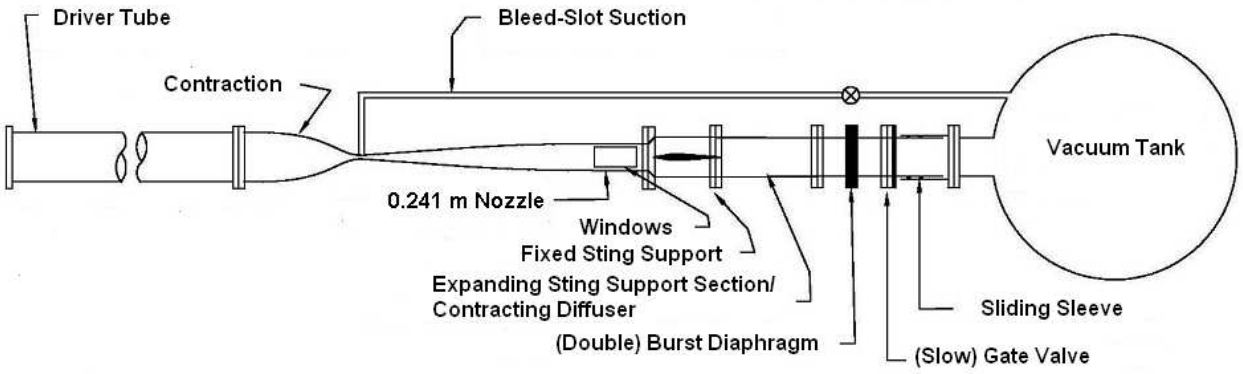

Figure 1: Boeing/AFOSR Mach-6 Quiet Tunnel Schematic

III. Tunnel Performance

The performance of the BAM6QT has continued to change over the past year. The status of quiet flow from January through June 2009 was reported in Reference 8. The maximum quiet pressure was above 163 psia.

A. Disruption of Quiet Flow

In October 2009 the diaphragms were accidentally burst without opening the gate valve (see Figure 1). This resulted in a shock traveling upstream into the nozzle, which likely loosened dust particles in the tunnel, or sent dust particles back upstream into the nozzle. Historically, this has caused a noticeable increase in the number of turbulent bursts,[9] and has even caused a period of a few weeks with either no quiet flow or a lowered maximum quiet pressure.[10] This time the result was a substantial increase in turbulent bursts, enough that a few runs immediately afterwards had no usable quiet flow time. After about ten runs at initial stagnation pressures higher than 140 psia, it was once again possible to get half-second segments of quiet flow without turbulent bursts at stagnation pressures above 160 psia.

Before the diaphragms were burst with the gate valve closed, additional measurements were taken for runs with initial stagnation pressures above 165 psia, using an XCQ-062-15A Kulite pressure transducer pitot probe. The BAM6QT's quiet performance is usually judged qualitatively using an uncalibrated hot-film array located on the nozzle wall. A Kulite pitot probe gives numerical results since it is calibrated, but the hot films are more convenient since they are non-intrusive and can be used simultaneously with other experiments. The probe was mounted on a traverse which allows axial and radial motion near the exit of the nozzle. There was no model in the tunnel for these runs and all measurements reported in this section were taken with the probe along the tunnel centerline at axial locations between 1.93 m and 2.39 m downstream of the throat.

A sample run from the summer of 2009 is shown in Figure 2. The initial stagnation pressure was $p_{0,i} = 178.3$ psia. The start-up effects end around $t = 0.05$ seconds. After start-up, the nozzle-wall boundary layer is turbulent for about 0.1 seconds. Then there is a period of intermittently quiet flow, consisting mainly of turbulent bursts, which are the large spikes seen in Figure 2. At about $t = 0.7$ seconds ($p_0 = 169$ psia) the flow is quiet for more than 0.1 seconds, followed by more quiet segments with frequent turbulent bursts. Each turbulent burst is approximately 1.5 ms long. The run ends around $t = 5.5$ sec ($p_0 = 123$ psia). After the first quiet segment there are more than 40 bursts during the run time, which is a large number, as will be discussed more later.

After the tunnel was again performing consistently, additional quiet flow data were examined from the hot films. Since the diaphragms were burst without opening the gate valve, the highest-pressure run that had a continuous second of quiet flow is shown in Figure 3, which shows a hot-film trace for a run with a 7° half-angle cone model with a 0.10 m base diameter installed in the tunnel at 6° angle of attack. This trace shows a maximum quiet pressure of $p_0 = 146$ psia. Also apparent in Figure 3 is an increase in noise after $t = 2$ seconds. This increase is only qualitative since the hot films are uncalibrated. This behavior has been

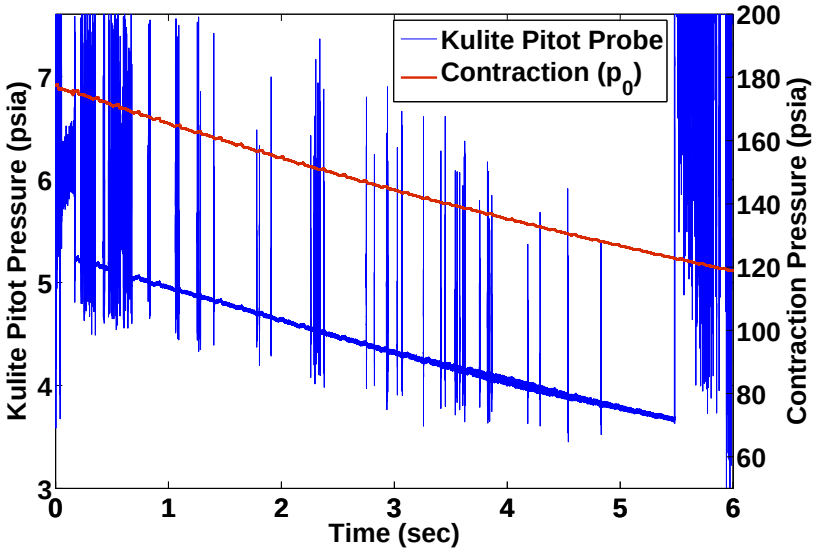

Figure 2: Trace from before the tunnel was run with gate valve closed. Kulite pitot probe trace plotted with contraction (stagnation) pressure. $p_{0,i} = 178$ psia, which is above the maximum quiet pressure. The Kulite trace (blue) is associated with the left-hand axis and the contraction trace (red) with the right-hand axis. The first significant quiet segment (longer than 0.1 seconds) is seen at $p_0 = 169$ psia, $t = 0.7$ sec. The probe was positioned 1.93 m downstream of the throat.

seen often in recent tests, although it is more noticeable in the hot-film data compared to the pitot probe. The pitot probe often also shows an increase in turbulent bursts near the end of high-pressure runs. The cause of this increase in noise is currently unknown.

In general, hot-film traces from after the tunnel was run with the gate valve closed show similar results to those from before. Short periods of quiet flow were sometimes seen above stagnation pressures of 170 psia, yet any operations above 160 psia had a large number of turbulent bursts and short segments of quiet flow, often less than 0.05 seconds each. The large number of turbulent bursts suggests that these higher pressures are not yielding fully quiet flow, but only intermittently quiet flow, and calls for further classification.

B. Defining Maximum Quiet Pressure

Periods of quiet flow at stagnation pressures above the previously-recorded maximum quiet pressure were seen during these tests. However, the segments had shorter durations and a higher number of turbulent bursts. It has been stated previously that the flow is quiet when $p_{02,RMS}/p_{02,mean}$ is about 0.06% or less, where $p_{02,mean}$ is the mean pitot pressure (total pressure behind the pitot shock) and $p_{02,RMS}$ is the RMS of the pitot pressure fluctuations.[11] This definition should be modified to specify the duration of quiet segments, due to the large number of turbulent bursts being seen at high pressures.

To determine how to classify this performance, it is noted that for several reasons periods of quiet flow need to be at least about 0.1 seconds long to be useful. Acquiring temperature-sensitive paint (TSP) data typically involves taking photographs with an exposure time of about 0.01 seconds at a rate near 20-30 Hz, or one photograph every 0.05 seconds. Additionally, many power spectral density (PSD) calculations performed by this research group use 0.1-second windows. However, the presence of useful segments of quiet flow does not necessarily mean the flow can be classified as quiet. It seems reasonable to define the maximum quiet pressure as the highest stagnation pressure at which there is one full second of quiet flow with less than 0.01 seconds of turbulent bursts. In other words, it is the pressure at which less than 1% of one second of "quiet" time is comprised of turbulent bursts.

By this definition, the maximum quiet pressure is currently 146 psia. Intermittently quiet flow has been observed at stagnation pressures as high as 169 psia. Above 169 psia, no useful quiet flow has been observed.

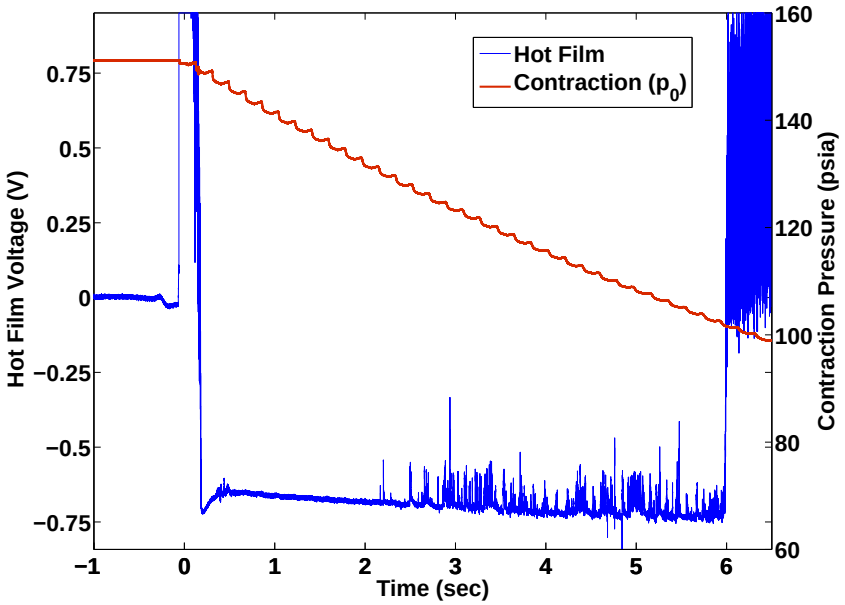

Figure 3: Uncalibrated hot-film trace plotted with contraction (stagnation) pressure near the maximum quiet pressure. $p_{0,i} = 149$ psia. There is a full second of quiet flow beginning at $p_0 = 146$ psia, (t=0.5 sec). The hot-film voltage (blue) is associated with the left-hand axis and the contraction pressure (red) with the right-hand axis. After start-up the nozzle-wall boundary layer is laminar and remains so until shut-down at $t = 6$ seconds. There is an increase in noise after $t = 2$ seconds for unknown reasons.

IV. Compression Cone Experiments with Nearly Sharp Nosetip

Design and testing of a 45-cm-long compression cone with a 3-m-circular-arc flare was conducted in the BAM6QT in the spring of 2009, with the goal of observing natural transition on an axisymmetric model under fully quiet flow.[8] The original design used a 1-mm-radius nosetip with an initial angle of 2°. Under quiet flow, the boundary layer was found to still be laminar at the back of the cone, where N was computed to be 13. A laminar boundary layer for N of at least 13 is surprising, especially since similar experiments by Blanchard on a compression cone detected transition at $N \approx 10$ [12, p.93], based on the point of maximum temperature. Balakumar and Kegerise[13] suggest that receptivity on a sharp cone provides larger initial amplitude waves than on a blunt cone. For this reason, it was proposed to test the same model with a sharp nosetip, in order to create more wave growth in an effort to observe natural transition under quiet flow.

There are a couple of important notes regarding Blanchard's experiments with respect to the experiments in this paper. The point of maximum temperature, which Blanchard chose as the 'transition point', would be near the end of the transitional region. Since transition occurs over a region, the choice of a single point is somewhat arbitrary. Here, the 'transition point' is chosen near the beginning of transition. Blanchard identifies the beginning of transition at $x \approx 27$ cm (11 in.) on his cooled-cone model in his Figure 5.1 [12, p. 66]. Referring to the computed N-factors shown in his Figure 7.3, this position corresponds to $N \approx 8$ [12, p. 96]. The back of Blanchard's model appears to have been under flow that was not fully quiet, with measured noise levels increasing at $x = 32$ cm (12.5 in.) [12, p. 36]. It is not clear to what extent this noise affected the results. Part of the motivation for the work presented here was to perform similar experiments to Blanchard, but with the entire model under quiet flow.

A. Construction of a Nearly Sharp Nosetip

A sharp nosetip was designed. However, the tip broke during fabrication so that the initial nosetip radius was 0.16 mm, as measured using a microscope camera. The initial angle of the tip was 1.5° after it had broken. This new nosetip was 17 cm in length and extended the compression cone's length to 47 cm.

Figure 4: Sharp nosetip for compression cone.

The first 2–3 cm of the nosetip was accidentally bent and re-straightened. The picture in Figure 4 shows the nosetip after it has been re-straightened. It is not known to what extent this defect affects these results.

B. Instrumentation

Pressure fluctuations were measured by PCB 132A31 sensors, which were placed in sensor ports located at distances of $x = 0.23$ m, 0.33 m, and 0.43 m from the nosetip of the cone. The PCB sensors are high-frequency piezoelectric pressure transducers with a resonant frequency above 1MHz. The sensors are high-pass filtered, and so only measure fluctuations above 11 kHz. They are designed as time-of-arrival sensors, and have not yet been recalibrated for measurements of weak pressure fluctuations. A Dantec type 55R47 hot-film sensor was placed at a position of $x = 0.459$ m from the nosetip. To visualize transition on the compression cone, the cone was first painted with an insulating layer of titanium dioxide powder mixed into ClearCote and then with a temperature-sensitive paint, a mixture of ClearCote and Tris(bipyridine)ruthenium(II) dichloride (Ru(Bpy)). Two blue LED arrays were used to excite the Ru(Bpy) crystals. Temperature-sensitive paint images were taken with a PCO.1600 camera with 2x2 binning. The pictures were taken at a frame rate of 28 Hz for images taken with the porthole windows and 27 Hz for the images taken with a large window. The rate was slower when using the large window due to the larger image size. The TSP data are to be calibrated for heat transfer, but remain qualitative for the present. The surface temperature is monotonic in heat transfer.

Data for the experiments were taken with one DPO7014-series and two DPO7054-series Tektronix Digital Phosphor Oscilloscopes. Data for the PCB sensors and the model hot-film were acquired for 10 s with a sampling rate of 2 MHz using Hi-Res mode. Data from 1 s before the run began were recorded for comparison to the flow-on pressure fluctuations. A contraction Kulite sensor was used to determine tunnel stagnation pressure. Two custom Senflex hot-films were used in conjunction with a Bruhn constant temperature anemometer to determine the length of the run as well as to qualitatively determine whether the flow was quiet or noisy.

C. Experimental Results

1. Comparison to Computations

The University of Minnesota's STABL software suite[14] was used to compute the growth of the second-mode waves using the parabolized stability equations. Results from the computations are compared to measured power spectra in Figures 5 and 6.

Figure 5a shows the power spectral density of PCB measurements made on a 7° half-angle straight cone.[15] The measurements for Figure 5a were made in the BAM6QT under noisy flow. The fluctuations measured by the PCB sensors are normalized by the mean surface pressure (edge pressure). Integration of the curve over a certain frequency range will give the RMS for that frequency range. Integration under the whole curve will give the total RMS. Note that these power spectral densities are plotted on a log scale. The mean surface pressure on the compression cone was found from calculations provided by the University of Minnesota.

The three spectra in Figure 5a show some of the different stages of transition, as measured by PCB-132A31 sensors. At $x = 0.208$ m, the spectrum shows laminar flow. This is evident from the pronounced decrease in noise as frequency increases. The prominent peak near 300 kHz is from the second-mode waves. At $x = 0.360$ m, the spectrum still shows laminar flow, but with large nonlinear second mode waves. The large peak at 200 kHz is the second-mode wave peak. The frequency of the second-mode waves has decreased due to the growth of the boundary layer. The peak at 400 kHz is from the harmonic of the second-mode waves. The presence of this peak indicates that the waves have become nonlinear. In addition, note that the fluctuations at all frequencies have become stronger. The final spectrum, at $x = 0.490$ m, shows turbulent

flow. The peak from the second-mode waves has disappeared, and there are significant fluctuations at all frequencies. The approximately exponential decrease in fluctuation strength with increasing frequency is characteristic of turbulent flows measured with PCBs.

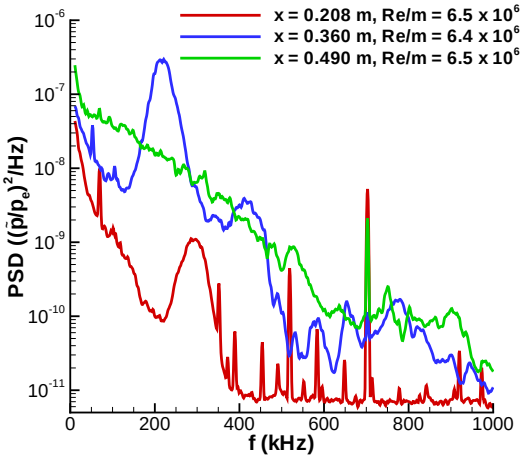

(a) Power spectra from the straight cone in Ref. 15.

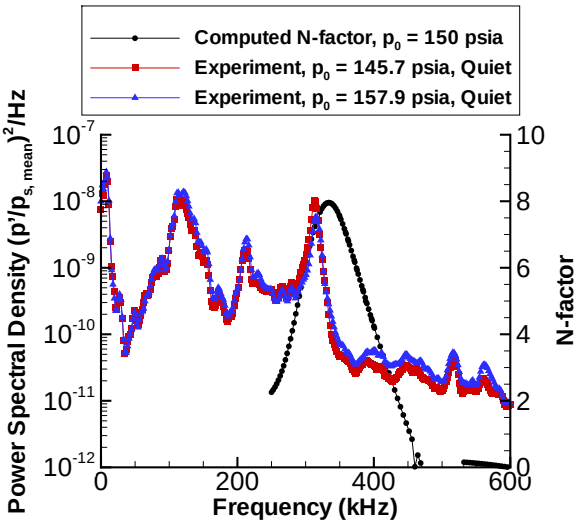

(b) Compression cone, $x = 0.23$ m

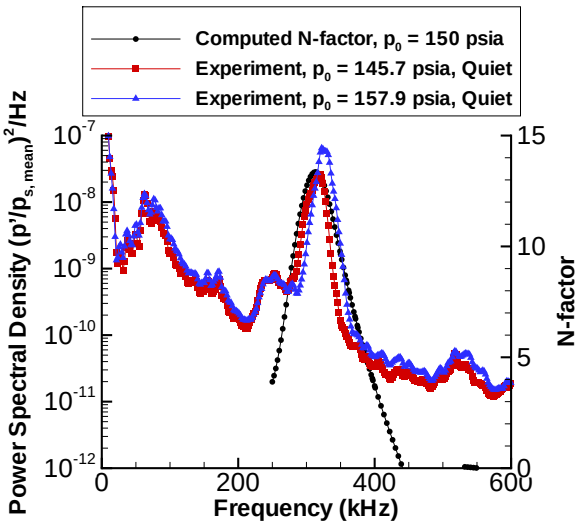

(c) Compression cone, $x = 0.33$ m

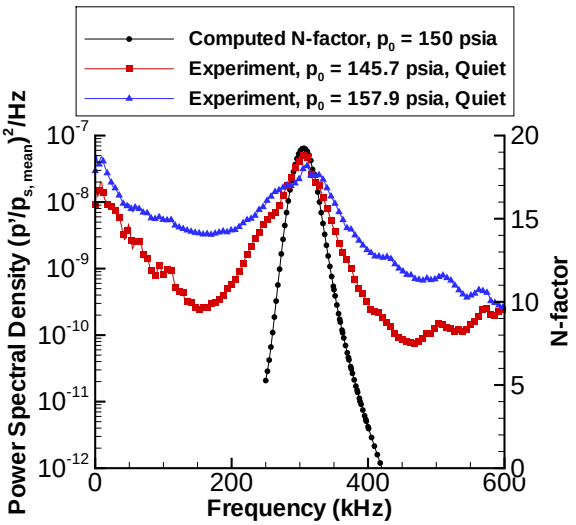

(d) Compression cone, $x = 0.43$ m

Figure 5: A comparison of computed N-factor to measured power spectra for quiet flow at $p_0 = 150$ psia. Note that since the PCBs need to be recalibrated, the magnitudes of the data can not be considered to be accurate. Peaks at 113 kHz at $x = 0.23$ m and 65 kHz at $x = 0.33$ m appear on all compression-cone runs. The cause of these peaks is unknown.

The rest of the plots in Figure 5 show comparisons between the computations and the experimental results at $p_0 = 145.7$ psia and $p_0 = 157.9$ psia. Nominally, $T_0 = 433$K and $T_w = 300$K for all of the compression cone measurements shown in this paper. The computations were performed for $p_0 = 150$ psia, $T_0 = 433$K, and $T_w = 300$K. The black dots show the N-factors computed for the amplified frequencies at the sensor locations. The computed peaks always coincide with a measured peak, and stay slightly above 300 kHz due to the nearly constant boundary layer thickness on the compression cone. The second-mode wave peaks are obvious in the measured spectra for $x = 0.33$ m and $x = 0.43$ m, but the large amounts of noise at $x = 0.23$ m make it difficult to find the second-mode wave peak without the computations.

At $x = 0.23$ m, the second-mode wave peak is small, making it likely that the waves are still laminar at

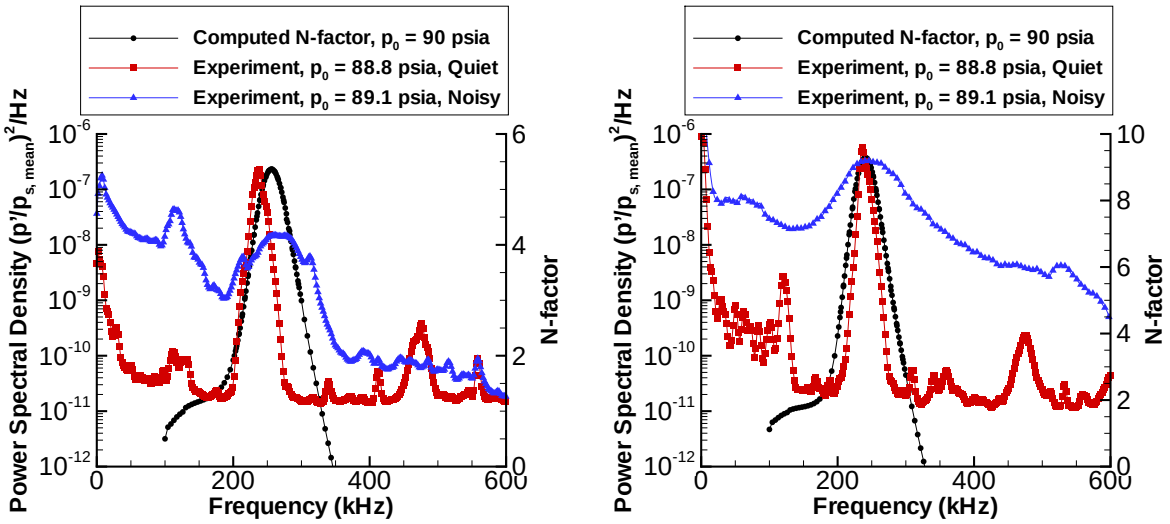

(a) $x = 0.23$ m

(b) $x = 0.33$ m

(c) $x = 0.43$ m

Figure 6: A comparison of computed N-factor to measured power spectra for quiet and noisy flow at $p_0 = 90$ psia. $M = 6.0$ for quiet runs and 5.8 for noisy runs.

this location. The waves are bigger at $x = 0.33$ m, but there is no evidence of increase at other frequencies, indicating that the waves are probably still linear. There is some difference between the two experimental spectra, due to their different pressures. At $x = 0.43$ m, it is difficult to tell from the PCBs whether or not transition has occurred for $p_0 = 157.9$ psia. While the second-mode wave peak is still clearly visible, the rest of the spectrum has filled out and appears to be very close to transition, if not already transitional. Nonlinear breakdown may be occurring at this location. The maximum PSD for the second-mode wave peak has decreased between $x = 0.33$ m and $x = 0.43$ m. This decrease also indicates that the flow is transitional or close to the onset of transition, since the peak must disappear as turbulence develops. For $p_0 = 145.7$ psia, the flow appears to be laminar, though the waves are nonlinear. Note the significant broadening of the second-mode wave peak, and the increase in fluctuations at low frequencies. Also, the computed N-factor for these waves is near 20, twice the expected N-factor for transition, and the flow is still laminar or transitional. At $x = 0.33$ m, the flow is clearly laminar at an N-factor of 13. These observations are supported by the TSP data, which allows determination of the transition location. It is unknown why laminar flow is able to persist to such high N-factors on this model.

The computed and measured peak frequencies of the second-mode waves were found to agree within 3.5% for $p_0 = 150$ psia and within 1.8% for $p_0 = 90$ psia. The computed and measured second-mode wave peak widths are different, especially at $x = 0.23$ m and $x = 0.43$ m. The widths agree well for $x = 0.33$ m. At $x = 0.43$ m, the difference is probably due primarily to the nonlinearity of the waves, which is not accounted for in the computations. The reason for the different widths at $x = 0.23$ m is unknown.

Figure 6 compares computed N-factors at $p_0 = 90$ psia to measurements at stagnation pressures close to 90 psia under both noisy and quiet flow. The flow is clearly laminar for all axial stations under quiet flow, with large second-mode waves visible near 240 kHz. What is likely a small harmonic is visible at 480 kHz. However, no growth in the second-mode waves is observed with increasing x. Laminar flow at unusually high N-factors is still observed. This problem has been encountered before on this model, and the reason for this lack of observed growth in the second-mode waves is still unknown.[8] The second-mode wave peak frequencies and peak widths show fairly good agreement between the computations and the quiet PSD spectra.

The second-mode wave peaks under noisy flow have very similar frequencies to those computed, though the widths differ. The flow appears laminar at $x = 0.23$ m, transitional or nearly transitional at $x = 0.33$ m, and turbulent at $x = 0.43$ m, with the second-mode wave peak having completely disappeared. The differences between the spectra under quiet flow and noisy flow illustrate the large effect of freestream noise on the development of second-mode waves. Note that waves are evident at N-factors close to 9 under noisy flow. This is again close to twice the expected N-factor for transition.

It is noted that some of the quiet-flow data included here were taken at pressures that are actually categorized as intermittently quiet flow. It is believed that these data are still useful, though, because they were taken from early in the runs, before any turbulent spots were seen in the wall hot films. Additionally, small numbers of turbulent spots did not appear to significantly affect the data. For these reasons, it is believed that the data presented here can be considered as having been taken under nominally quiet flow. However, it is important to note that the freestream noise level of the flow at the back of the cone needs to be measured to confirm that it is quiet, especially near 160 psia. The flow is nominally quiet to the end of the nozzle, but this may not be true when the flow is intermittently quiet.

2. TSP Measurements & Observation of Hot Streaks Under Quiet Flow

Figures 7 and 8 show TSP data taken under quiet and noisy flow, respectively. The images show the surface temperature change with respect to the surface temperature before the run. The TSP images for $p_0 = 88.8$ psia under quiet flow (Figure 7a) show low, uniform heating, indicating that the flow is laminar over the entire model. Hot streaks appear at the end of the model when $p_0 = 135.1$ psia, starting at about 0.41 m from the nosetip (Figure 7b). The hot streaks weaken, but persist to the end of the cone. For $p_0 = 157.9$ psia, the hot streaks start at 0.36 m, weaken starting at 0.40 m, and then strengthen again at 0.44 m.

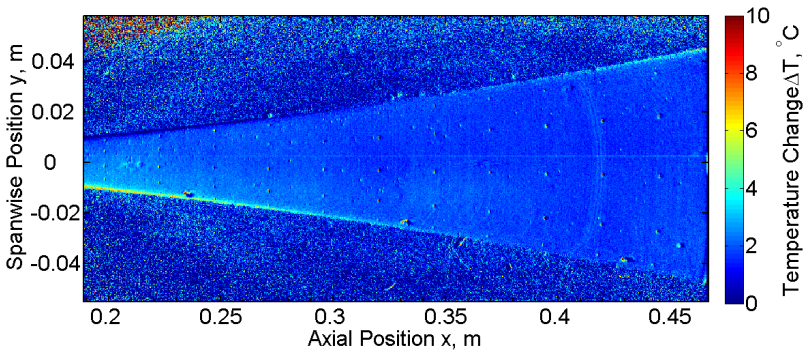

(a) $p_0 = 88.8$ psia

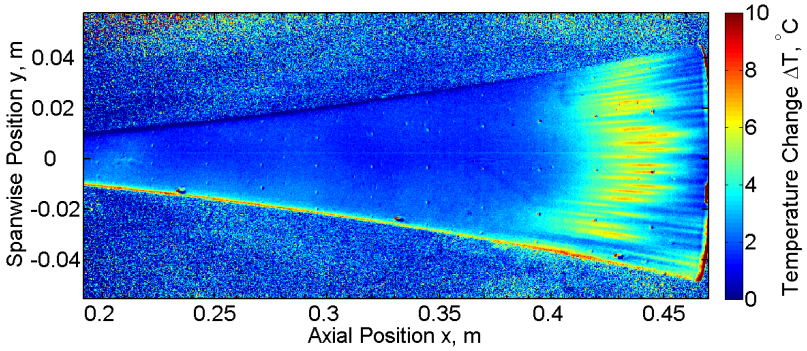

(b) $p_0 = 135.1$ psia

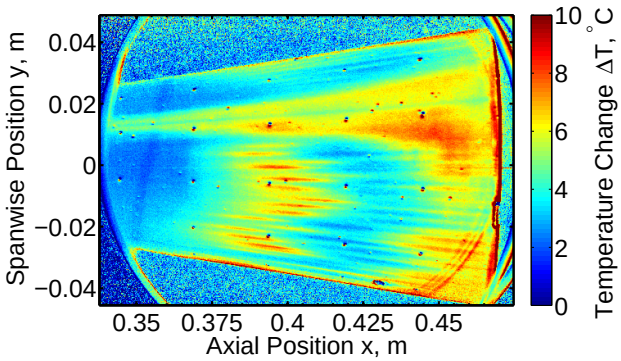

(c) $p_0 = 157.9$ psia

Figure 7: Temperature-sensitive paint images corresponding with selected runs in Figure 9. The image in Figure 7c is smaller because a smaller window had to be used to accommodate the higher pressure. Flow is from left to right.

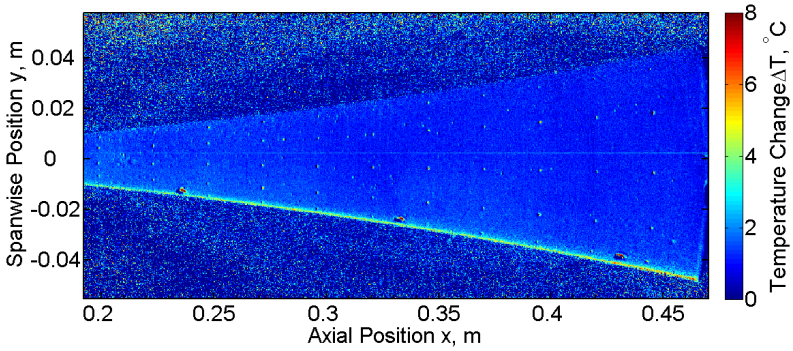

(a) $p_0 = 40.4$ psia

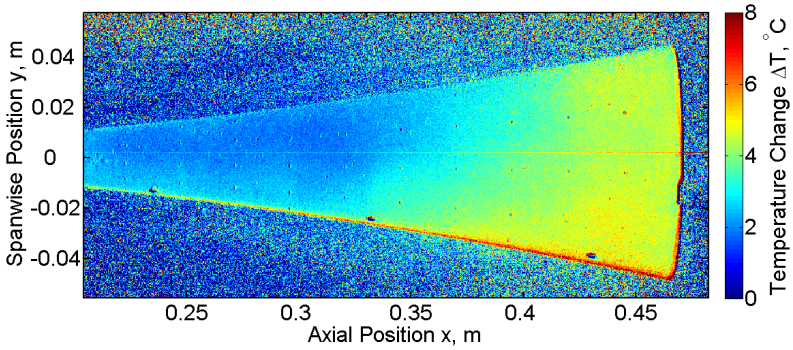

(b) $p_0 = 89.1$ psia

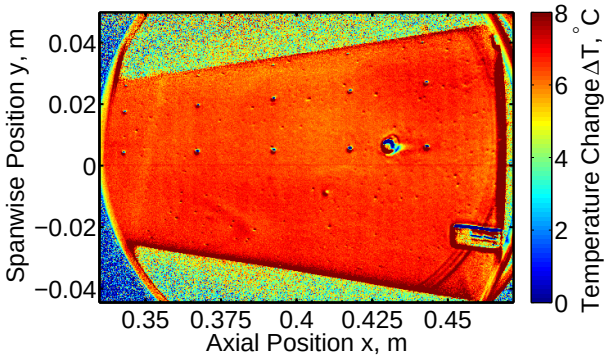

(c) $p_0 = 228.0$ psia

Figure 8: TSP images corresponding with selected runs in Figure 10. The image in Figure 8c is smaller because a smaller window had to be used to accommodate the higher pressure. Flow is from left to right.

When hot streaks appear, there are on average eight streaks for every 30° about the circumference of the compression cone, regardless of pressure. Figure 7c shows that the hot streaks move forward with increased stagnation pressure. The two hot streaks at $y \approx 0.025$ m in Figure 7c were caused by an unusually large flaw in the paint that was identified at the upstream end of the cone. Note that these hot streaks extend much further forward on the cone than the rest. The streaks also strongly resemble transition behind an isolated roughness element, as in Reference 16. These two streaks from the wake of the paint flaw become turbulent, as evidenced by the spreading of the streaks.

Figure 8 shows TSP data taken under noisy flow. These images show completely laminar flow on the surface of the cone at $p_0 = 40.5$ psia (Figure 8a). Transition is evident at $p_0 = 89.1$ psia (Figure 8b), as shown by the increase in heating starting near $x = 0.34$ m. Turbulent flow is observed along the entire visible length of the cone at $p_0 = 228.8$ psia, as shown by the uniformly high temperatures (Figure 8c). Higher stagnation pressures lead to more turbulence, as expected. It is important to note that no streaks are observed during transition under noisy flow, consistent with previous results.[16]

The hot streaks seen on the compression cone in quiet flow may be due to either Görtler vortices, an interaction between Görtler vortices and second-mode waves, or a secondary instability of the second-mode waves. Blanchard speculated that the secondary instability may be an azimuthal mode, which is consistent with these results [12, pp. 87-88]. It is unknown why the hot streaks sometimes weaken and then strengthen again as x increases. Weakening of the streaks would be expected if the laminar boundary layer were growing, but the laminar boundary layer thickness should be constant on this model, according to computations. The constant thickness of the boundary layer is confirmed by the constant frequency of the second-mode waves, which is linked to the boundary layer thickness.[17] Transition may be the cause of the re-strengthening of the streaks, since it would cause an increase in heating. The PCB data provide some support for this idea. It is unknown why the streaks appear under quiet flow and not noisy flow.

3. Comparison of TSP and PCB Data

Figure 9 shows the corresponding PCB data for the TSP data presented above. Power spectra are shown for all three axial positions measured. The 'Pre-Run' spectra show the measured fluctuations for each sensor before the tunnel was started. These fluctuations are primarily due to background electrical noise.

For $p_0 = 88.8$ psia, the PCB sensors confirm that the flow is laminar, since prominent second-mode wave peaks are visible near 220 kHz at all positions. The spectra for $p_0 = 135.1$ psia also indicate laminar flow at all positions. At this pressure, streaks are observed to appear near the back of the cone, extending to positions in front of the sensor at $x = 0.43$ m. While the second-mode wave peak near 300 kHz is observed to grow with increasing x, the only major qualitative change in the spectra is the appearance of an additional peak near 600 kHz. This peak is presumably a harmonic of the second-mode waves, since it occurs at frequencies near twice the fundamental frequency. This harmonic is seen after the streaks appear, giving some support to the idea that the streaks are related to nonlinearities of the second-mode waves. However, more measurements are needed to confirm such a relation.

For $p_0 = 157.9$ psia, the spectra appear laminar up until $x = 0.43$ m, at which point the flow appears to be transitional or turbulent. This is shown both by the shape of the curve and the fact that the peak level is lower at $x = 0.43$ m than at $x = 0.33$ m. At $x = 0.43$ m, the streaks are observed to be weakened and beginning to strengthen again (see Figure 11a). The fact that the PCB data show transitional flow at this point suggests that the re-strengthening of the streaks is due to transition. More measurements are needed to confirm this.

Some problems with the PCB sensors are observed at lower quiet pressures, as in the $p_0 = 88.8$ psia case (Figure 9a), where the sensors do not show growth in the second-mode waves with increase in downstream position and the amplitude appears to be large compared to wave amplitudes at higher pressures. Additionally, a peak at 113 kHz was seen in the first sensor for all runs. Similarly, a 65 kHz peak was also seen in the second sensor for some but not all of the runs. The causes of these peaks are unknown.

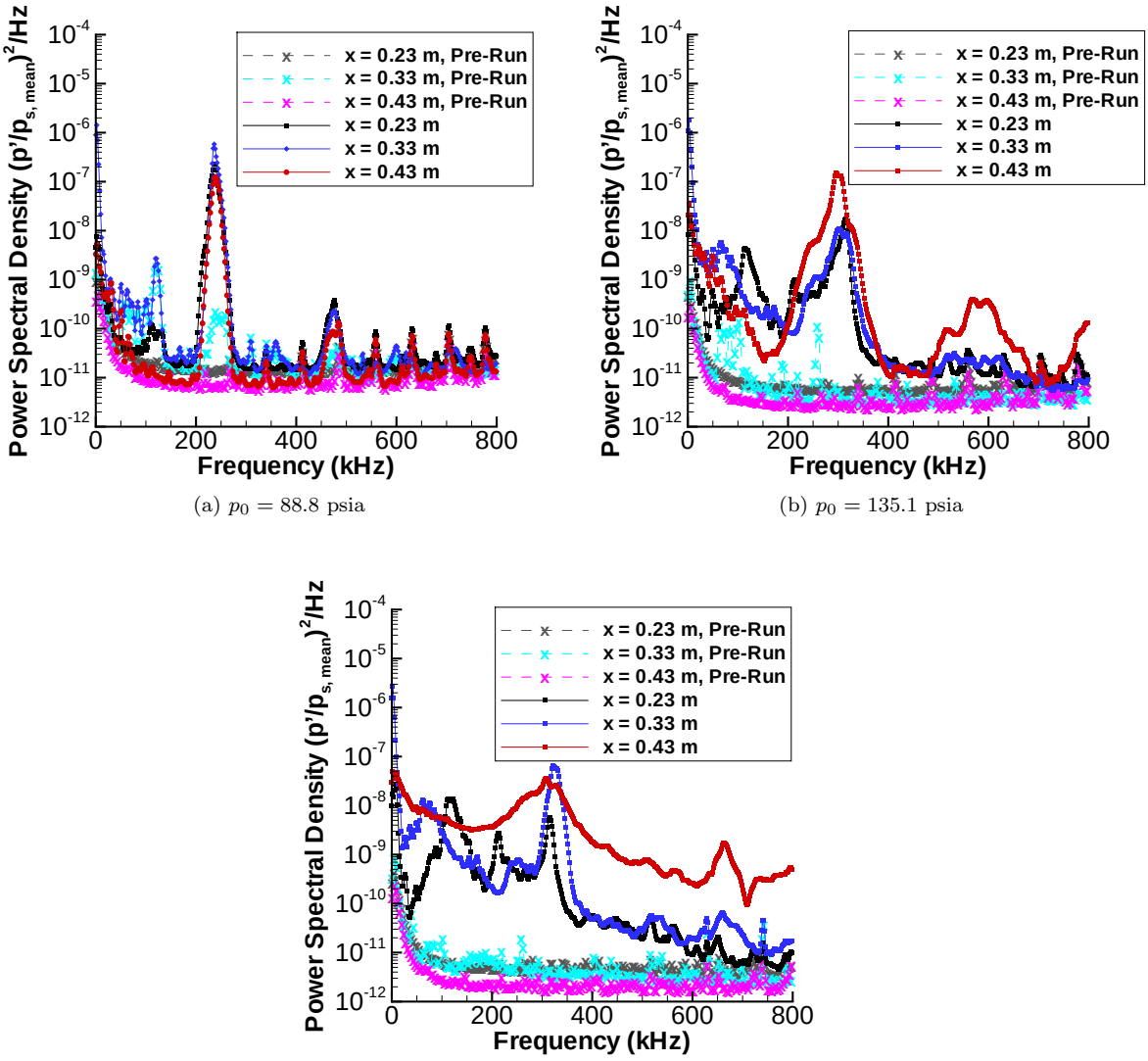

(a) $p_0 = 88.8$ psia

(b) $p_0 = 135.1$ psia

(c) $p_0 = 157.9$ psia

Figure 9: Power spectra of the PCB 132A31 sensor readings under quiet flow.

Figure 10 shows PCB data under noisy flow. For $p_0 = 40.5$ psia (Figure 10a), the flow is confirmed to be laminar. Some growth of the second-mode waves near 200 kHz is observed. The breakdown to turbulence of the second-mode waves is observed at $p_0 = 89.1$ psia (Figure 10b). The second-mode wave peak is near 250 kHz. Note that the peak has completely disappeared by $x = 0.43$ m. Since the flow is completely laminar at this pressure under quiet flow, the noise level of the tunnel is observed to have a large effect on the second-mode waves. At $p_0 = 228.8$ psia, the flow is turbulent at each sensor. The PCB data under noisy flow do not seem to indicate any differences in the breakdown process from that under quiet flow, offering little information as to why the streaks do not appear under noisy flow.

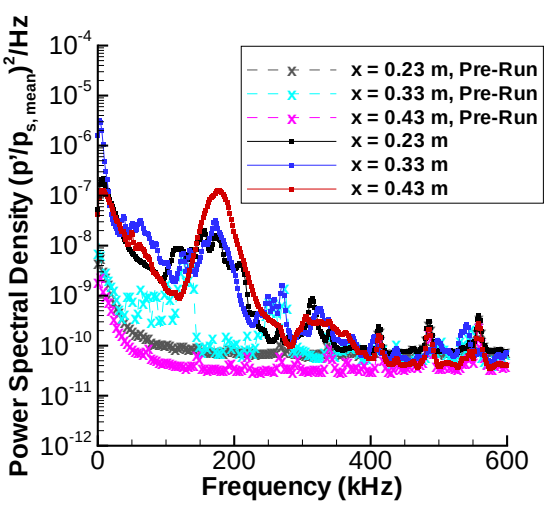

(a) $p_0 = 40.5$ psia

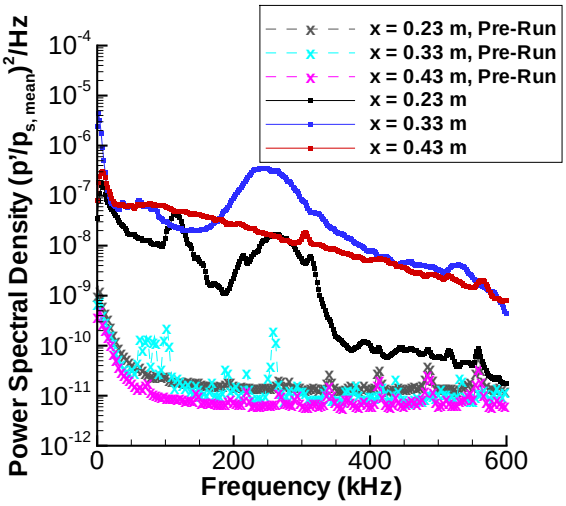

(b) $p_0 = 89.1$ psia

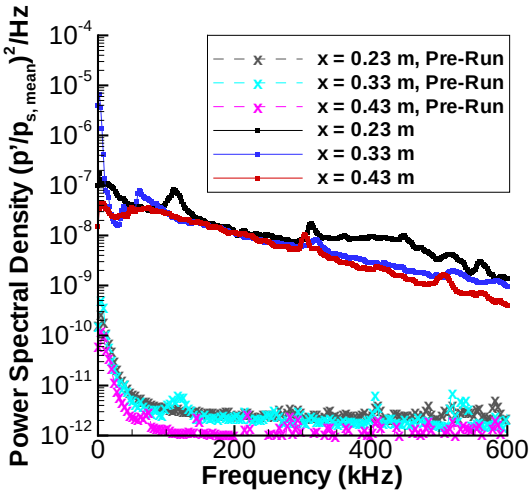

(c) $p_0 = 228.8$ psia

Figure 10: Power spectra of the PCB 132A31 sensor readings in noisy flow.

4. N-Factor at Transition Onset

The computations make it possible to find the N-factor at which transition occurs. Since the streaks appear to be turbulent when they re-strengthen, the point at which this re-strengthening begins was assumed to indicate transition onset. In a streamwise temperature profile, this corresponds to the local minimum after the streaks first appear. For the noisy case, a different assumption had to be made, since the streaks do not appear under noisy flow. For noisy flow, the transition onset was assumed to occur at the point at which

the surface temperature begins to increase. Computations predict that the laminar heat transfer should be nearly constant, due to the nearly constant thickness of the boundary layer. A significant increase in heating should thus be due to transition.

Figure 11 shows streamwise temperature profiles from the TSP data compared to the computed wall heat flux. Heat flux could not be calculated from the TSP data due to the lack of a reference heat transfer measurement anywhere on the surface. Figure 12 shows the computed N-factors for both a $p_0 \approx 90$ psia case and $p_0 \approx 150$ psia case. In Figure 11a, the temperature increases, decreases, and begins to increase again as the streaks reappear. The first increase is the first appearance of the streaks, which occurs at $x = 0.361$ m, where $N \approx 15$. The second increase indicates transition, and occurs at $x = 0.428$ m, which corresponds to an N-factor of 19. In Figure 11b, the temperature begins to increase at $x = 0.321$ m, corresponding to an N-factor of 9. These N-factors are both much higher than the typically expected values. It is not clear why this is the case. It is not entirely certain that the temperature profile in Figure 11a follows the expected laminar profile before the appearance of the streaks, since not much of the laminar region was observed. This is due to the small size of the window. However, it seems likely that this is the case, given the other observations made with the large window, and the fact that the PCBs show laminar flow forward of the third position for this condition. Further measurements are necessary to confirm that this is true.

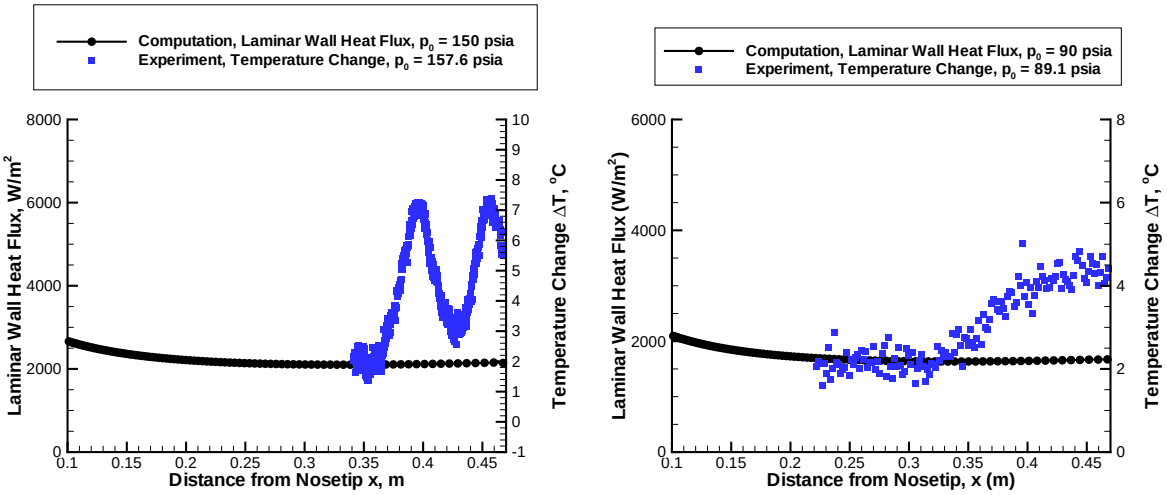

(a) Quiet flow, $p_0 = 150$ psia

(b) Noisy flow, $p_0 = 90$ psia

Figure 11: Streamwise temperature profiles from TSP data compared to wall heat flux computations. Transition is observed in both quiet and noisy cases, defined in the quiet case as the point where the second increase in temperature begins, and in the noisy case as the point at which temperature begins to increase.

5. Detection of Second-Mode Waves Using Hot Films

Figure 13 shows power spectra computed from the hot-film data. Hot films typically cannot detect second-mode waves, due to their low frequency response. However, on this model, large, relatively low-frequency waves can be obtained, since large waves can be obtained at low pressures. Figure 13 shows comparisons between power spectra from PCB sensors and hot films. For $p_0 = 40.5$ psia under noisy flow, the waves are near 200 kHz. They are clearly visible in the PCB spectrum, and faintly visible with the hot film. For $p_0 = 88.8$ psia under quiet flow, the situation is similar. The second-mode wave peak is larger on the hot film under these conditions, but it is very close to a peak due to electrical noise, making it less clearly visible.

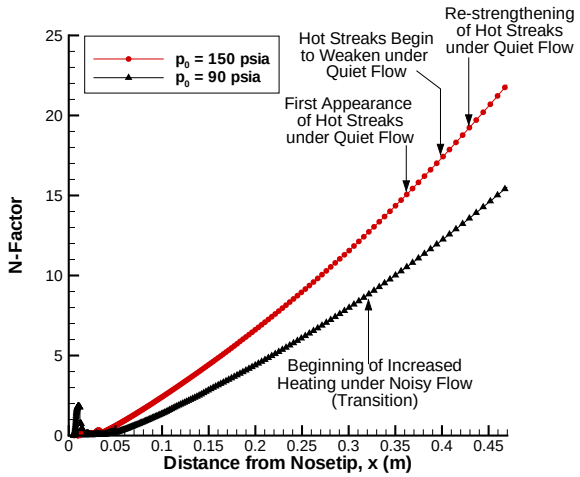

Figure 12: Computed N-factors for $p_0 = 150$ psia and $p_0 = 90$ psia

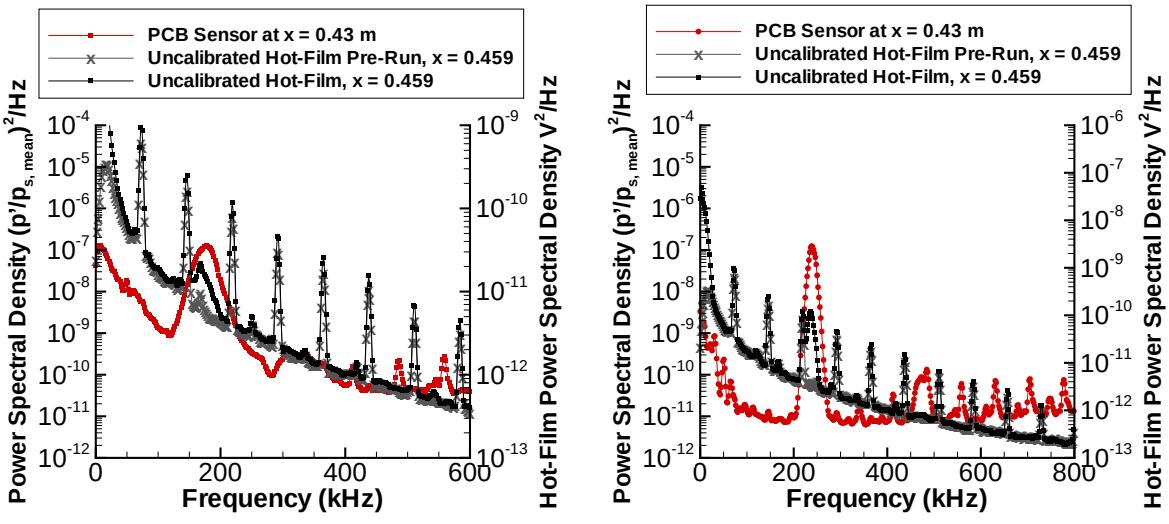

(a) Noisy flow, $p_0 = 40.5$ psia

(b) Quiet flow, $p_0 = 88.8$ psia

Figure 13: Comparisons of power spectra from PCB sensors and the model hot film, showing that second-mode waves are sometimes visible on the hot films.

D. Future Work

Future tests on the compression cone should repeat runs at $p_0 = 150$ psia and $p_0 = 90$ psia and several pressures in between. Additional TSP images should be obtained to better understand the correlation between the hot streaks and the pressure fluctuations. Additional sensor positions should be added to reduce the spacing between the PCB sensors, especially in the region where the hot streaks appear. Another type of sensor, such as a hot wire or laser differential interferometer, should be used to check the data from the PCBs. Quantitative heat transfer data should also be obtained by installing heat transfer gages and thermocouples on the model. A better calibration of the PCBs needs to be done in order to obtain more reliable measurements of the pressure fluctuations on the surface of the cone. Further measurements of the noise level in the tunnel should also be performed in order to determine the extent of the quiet core in the BAM6QT and whether or not the flow impinging on the back of the cone is quiet. In addition, if the entire cone is under quiet flow, tests with the cone positioned farther upstream should show the streaks appearing in the same streamwise positions. Such tests should be performed. Another compression cone should be designed to achieve higher N-factors so that transition can be observed closer to the front of the model and at lower pressures.

V. Crossflow Instability and Transition on a Cone at Angle of Attack

The crossflow instability is likely to be critical on many hypersonic vehicles, yet it is poorly understood.[2] Measurements on a cone at angle of attack have visualized the stationary crossflow waves, but much remains uncertain regarding the effect of tunnel noise on the crossflow instability.[18] In an effort to continue the work begun by Swanson,[18] experiments have been performed in the Boeing/AFOSR Mach-6 Quiet Tunnel on a 7° half-angle cone at 6° angle of attack to visualize the effect of tunnel noise and distributed roughness on the crossflow instability. The cone used is 0.41 meters long with a nominally sharp nosetip, and a base diameter of 0.10 meters. Temperature-sensitive paints were used to provide a global temperature distribution and to visualize flow structures. In future experiments, hot wires and heat-flux gages will also be used.

A. Surface Characteristics

Three test cases have been performed, two with a smooth paint finish (Cases 1 and 2), and one with a rough paint finish (Case 3). Some of the characteristics of the paint finish can be found in Table 1. Roughness measurements were taken by traversing a Mitutoyo Surftest SJ-301 profilometer over a 4 mm length. The average roughness value was found along the model's surface by averaging the profilometer readings at three random locations. Paint was only applied to the frustum of the cone, creating a step where the nose meets the frustum. The step in the paint was also measured with the profilometer. The average roughness between the two smooth paint finishes are similar, and almost eight times less than the rough finish case. The initial step in the paint is nearly the same in the three cases, and this step in the paint did not appear to have a significant effect. This was checked by observing the upstream portion of the cone at various freestream Reynolds numbers. An example is shown in Figure 14 where the entire frustum of the cone is pictured. The step in the paint causes a slight rise in temperature, but any disturbances appear to ultimately be suppressed. Several images of the surface under the microscope with a scale are shown in Figure 15.

Case	Step in the paint [μm]	Average Roughness [μm]
1	78	0.25
2	69	0.18
3	81	1.98

Table 1: Surface characteristics of the three paint finishes

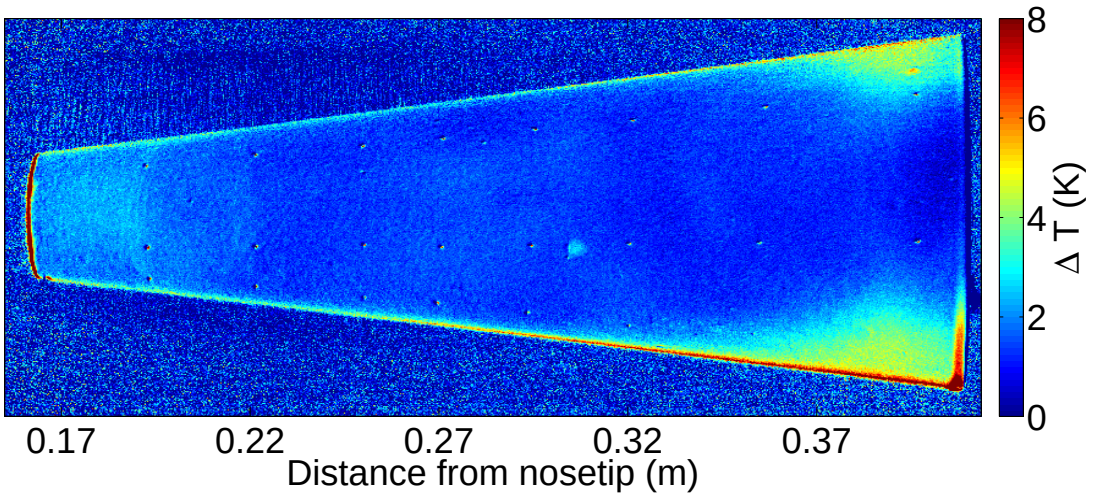

Figure 14: Visualization of the effect of the step in the paint on the flow field. $Re_\infty = 9.4 \times 10^6$/m, $p_0 =$ 105 psia, $T_0 = 403$ K

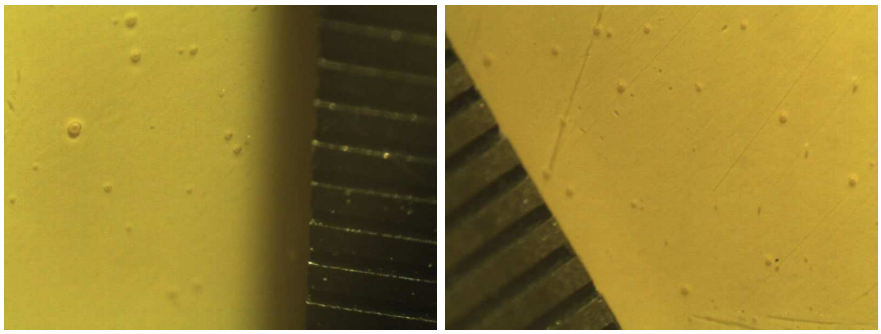

(a) Smooth paint finish, Case 1

(b) Smooth paint finish, Case 2

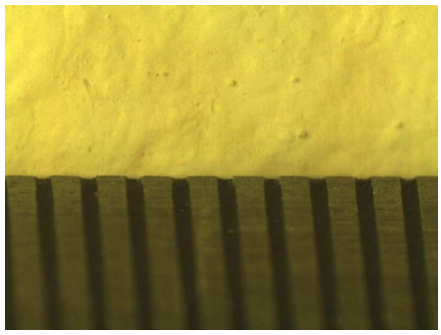

(c) Rough paint finish, Case 3

Figure 15: Microscope images of the paint finish, ruler markings 0.4 mm ($\frac{1}{64}$") apart

B. Tunnel Noise Effect

Measurements were taken for a rough paint finish (Case 3, Figure 16) and a smooth paint finish (Case 1, Figure 17) at a freestream unit Reynolds number of 11 $\times$ 10^6/m under noisy and quiet flow. ΔT refers to the number of degrees Kelvin above the pre-run temperature. The cone is shown from the side in both figures. Both of the paint finishes show that under these flow conditions and for this model, tunnel noise has a substantial effect on the crossflow vortices. Under noisy flow, the rough paint finish (Case 3, Figure 16)

shows transitional or turbulent flow at the rear of the cone towards the windward ray. Under quiet flow, the crossflow vortices are apparent, but have not started to break down to turbulence. 11 vortices are visible at the downstream end of the cone. Similar results were obtained for a unit Reynolds number of 8.0×10^6/m and 9.0×10^6/m with the same rough paint finish.

The smooth paint finish (Case 1, Figure 17) also shows an effect of tunnel noise. Under noisy flow, the region of high temperature indicates transitional flow. The temperature is cooler downstream of this transitional flow because the heat transfer drops as the turbulent boundary layer grows. Due to the poor signal to noise ratio of the paints for this specific case, it cannot be said with certainty that this is in fact turbulent flow downstream of the high temperature streak because there could be some laminar structures that cannot be resolved. Under quiet flow, the crossflow vortices are apparent and do not begin to break down. There are roughly 8 vortices visible at the base of the cone. As in the rough paint case, the noise appears to be inducing turbulent flow. The smooth paint finish for Case 1 did not show a significant effect of tunnel noise for a Reynolds number of 8.0×10^6/m (fully laminar under noisy and quiet flow), and no runs were performed at a Reynolds number of 9.0×10^6/m. The smooth paint finish for Case 2 (not shown here) showed an effect of tunnel noise for $Re_\infty = 8.0\times 10^6$/m, 9.0×10^6/m and 11×10^6/m, similar to the rough paint finish. There is no obvious effect of the distributed roughness on the flowfield for these specific conditions shown. This will be discussed in more detail in the next section.

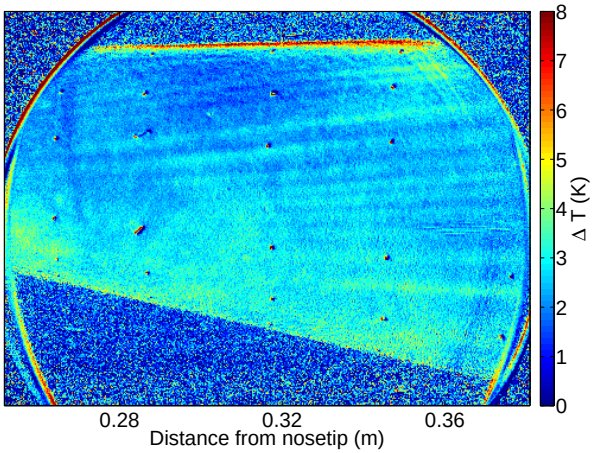

(a) Quiet flow, $p_0 = 145$ psia, $T_0 = 429$ K

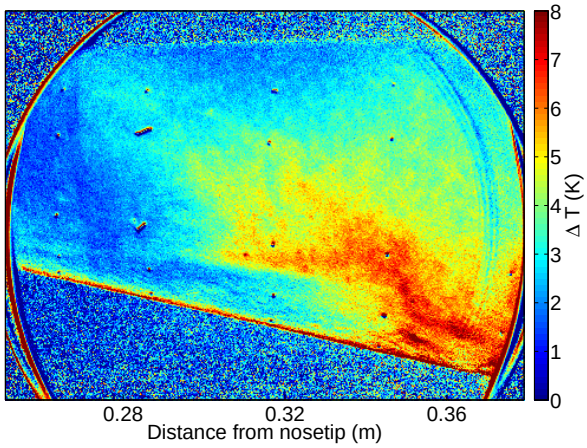

(b) Noisy flow $p_0 = 130$ psia, $T_0 = 416$ K

Figure 16: Temperature-sensitive paint images for rough paint finish (Case 3), $Re_\infty = 11 \times 10^6$/m, side view of the cone. Flow is from left to right.

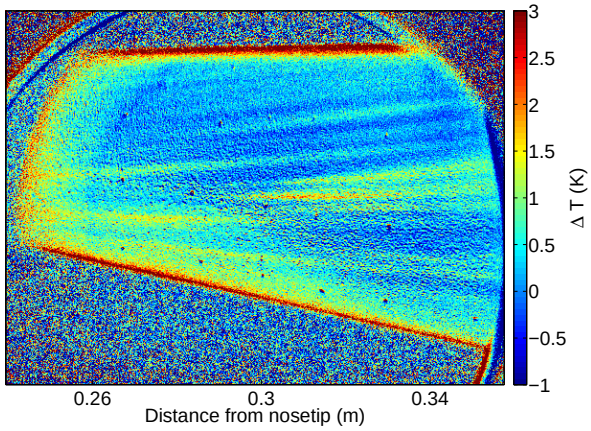

(a) Quiet flow, $p_0 = 144$ psia, $T_0 = 426$ K

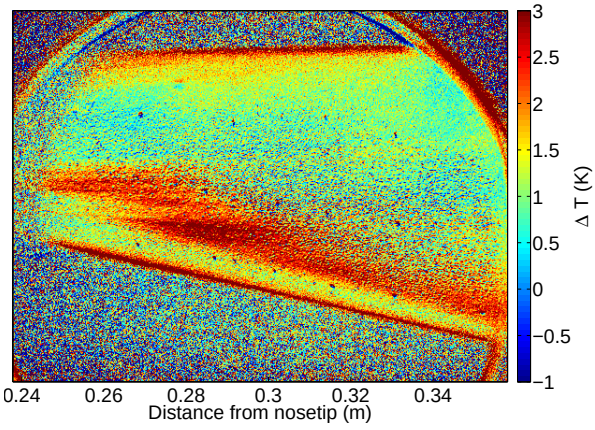

(b) Noisy flow, $p_0 = 127$ psia, $T_0 = 412$ K

Figure 17: Temperature-sensitive paint images for smooth paint finish (Case 1), $Re_\infty = 11 \times 10^6$/m, side view of the cone. Flow is from left to right.

C. Distributed Roughness Effect

Figure 18 shows the two smooth paint cases and the rough paint case at the same Reynolds number (11×10^6/m) under noisy flow. The second smooth case (Case 2) and the rough case show the transition front moving towards the windward ray from the sides. The first smooth case (Case 1) shows what appears to be transitional or turbulent flow along the lower part of the image, and potentially a turbulent boundary layer at the very top portion of the cone near the base. Note that the temperature scale is finer in Case 1 than the other cases. There appears to be no substantial effect of the distributed roughness under these conditions. All three cases show a transition front moving from the sides to the windward rays, with the only difference being the asymmetry seen in Case 1. This asymmetry could have been caused by a slight error in positioning the model such that the full windward portion was not in view.

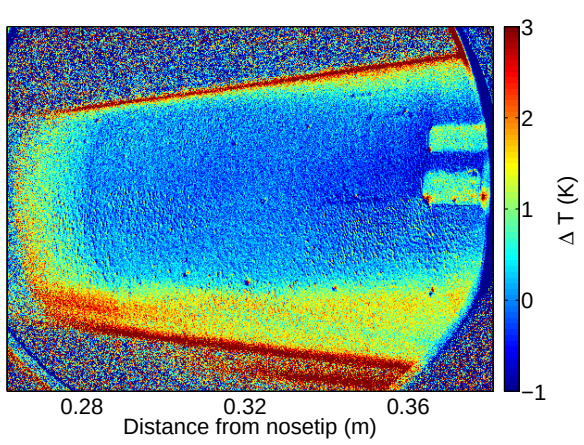

(a) Smooth paint finish, Case 1, $p_0 = 128$ psia, $T_0 = 414$ K

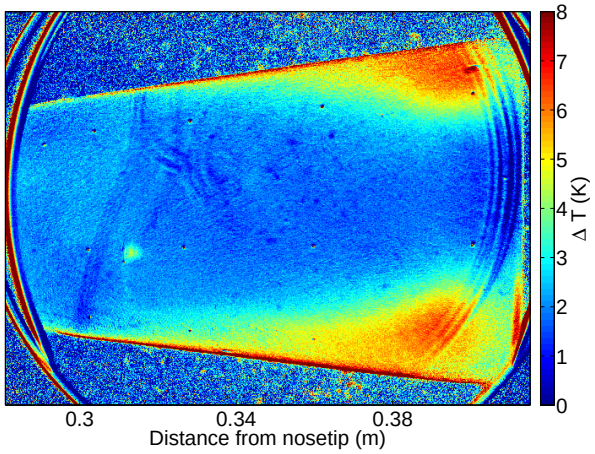

(b) Smooth paint finish, Case 2, $p_0 = 127$ psia, $T_0 = 413$ K

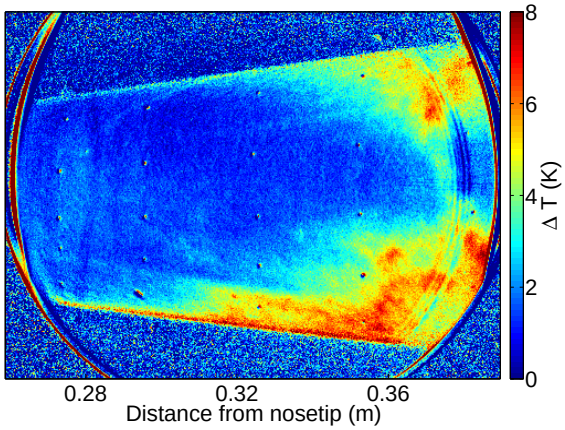

(c) Rough paint finish, Case 3, $p_0 = 128$ psia, $T_0 = 414$ K

Figure 18: Temperature-sensitive paints images for rough and smooth paint finish, noisy flow, $Re_\infty = 11 \times 10^6$/m, windward view of the cone. Note the difference in the temperature scale for the different cases. Flow is from left to right.

At a lower freestream Reynolds number, the effect of the distributed roughness has a more profound effect. Figure 19 shows the three cases at a Reynolds number of 9×10^6/m under noisy flow. Figure 20 shows the same data as Figure 19a with a finer temperature scale. The smooth paint finish (Case 2) and the rough paint finish (Case 3) show similar trends. The transition front is moving from the side to the windward ray. This was the same trend shown for a freestream Reynolds number of 11×10^6/m. The Case 1 smooth paint finish shows what may be transitional flow near the windward ray, but crossflow vortices are visible and the boundary layer is still laminar closer to the leeward ray towards the base of the cone. There is a substantial difference between the first and second smooth cases, despite the fact that the average

roughness of the paint is similar. It can then be inferred that the average roughness is not the only factor that determines the effect of the surface roughness on the boundary layer. The spatial frequency and spatial distribution of the roughness almost certainly have a substantial effect.

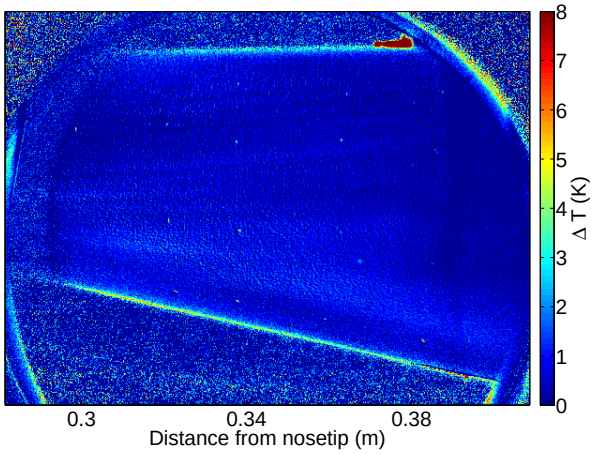

(a) Smooth paint finish, Case 1, $p_0 = 105$ psia, $T_0 = 412$ K

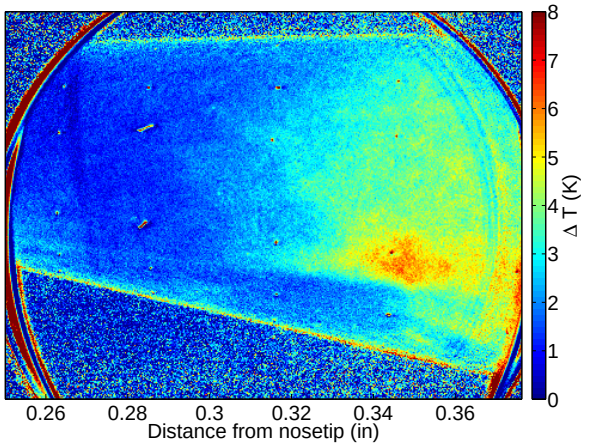

(b) Smooth paint finish, Case 2, $p_0 = 109$ psia, $T_0 = 422$ K

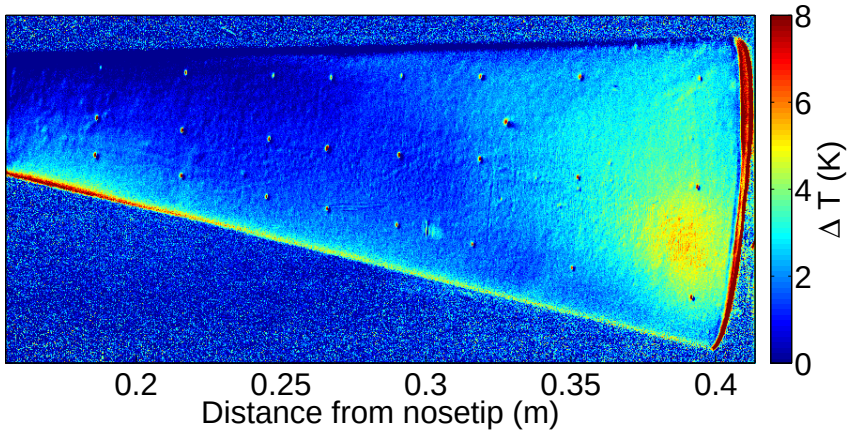

(c) Rough paint finish, Case 3, $p_0 = 108$ psia, $T_0 = 421$ K

Figure 19: Temperature-sensitive paints images for rough and smooth paint finish, noisy flow, $\mathrm{Re}_\infty = 9{\times}10^6$/m, side view of the cone. Flow is from left to right.

Figure 21 plots the mean-square spatial spectra for the two smooth cases. The window size was 1000 points, and the profilometer sampled at 2000 points per millimeter, so the spectra is only capturing short wavelengths of less than 0.5 mm. The MATLAB mean-square spectrum function (msspectrum) was used in the calculations. Three different spatial spectra taken at random locations were averaged to produce the plots. In hindsight, it would have been better to have more profilometer measurements, but the Case 1 paint finish was removed before it was realized what sort of impact the spatial frequency of the roughness could have on the boundary layer. Some differences in the frequency distribution of the roughness are evident. It may be that these details have an effect on the crossflow vortices. Clearly, many more roughness measurements are needed. These should include measurements over longer distances to better capture the longer wavelengths that are likely to be the most important. The regions of the cone surface where the roughness is most important also remain to be determined.

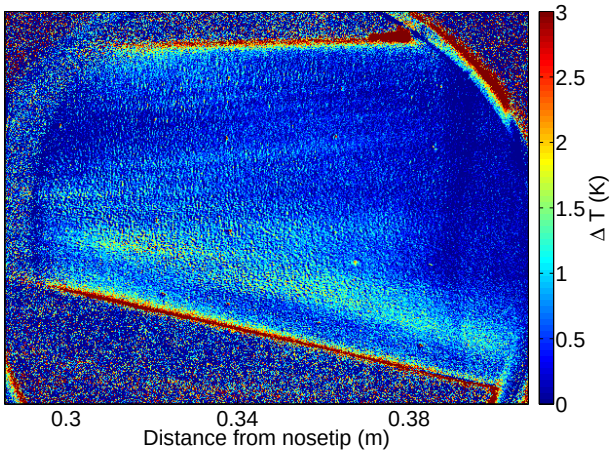

Figure 20: Same image as Figure 19a with a finer temperature scale. Flow is from left to right.

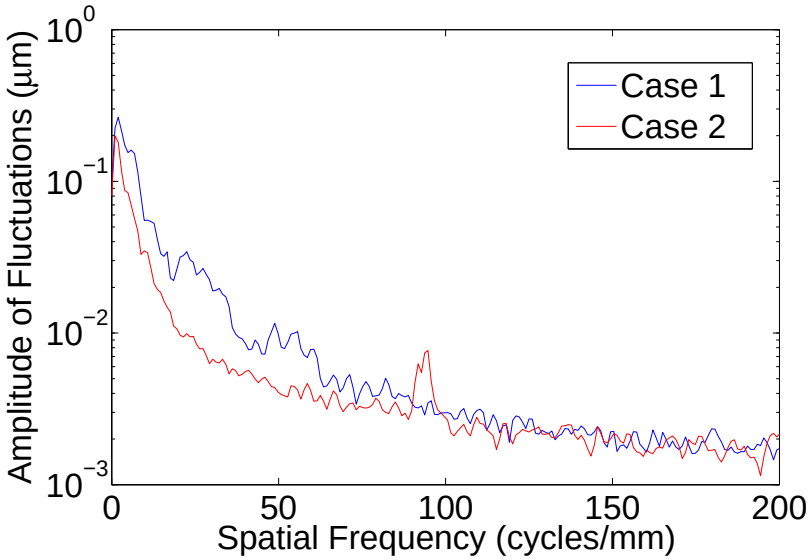

Figure 21: Mean-square spatial spectra for the two smooth paint finishes.

VI. Effect of Tunnel Noise on Laminar Stagnation Point Heating

A. Background

Stagnation point heating rates that are augmented above predicted values have been seen in a number of experiments and facilities over the past few decades. Holden[19] studied heating augmentation resulting from particulate interaction with the bow shock of blunt models. Hoshizaki[20] reported on several mechanisms thought to cause increased heating, including freestream turbulence. More recently, experiments with CEV (Crew Exploration Vehicle) and capsule models have shown unexpected increases in heat transfer rate in excess of 10% above predictions near the stagnation point region under laminar conditions.[21,22] While tunnel noise is commonly cited as a potential cause of heating augmentation, little work has been done to show a correlation. The present study seeks to determine whether a relationship exists between tunnel noise and stagnation point heating. The study was conducted on a hemisphere in both quiet and noisy flow in the BAM6QT.

B. Experimental Setup and Data Acquisition

A 3.60-cm (1.414-in.) diameter stainless-steel hemisphere was assembled at AEDC Tunnel 9 and shipped to Purdue to be run in the BAM6QT. Seven custom AEDC Schmidt-Boelter gages were installed, one at the stagnation point and 6 more at ±30, ±60, and ±90 degrees along a surface ray. The gages were calibrated in the AEDC Aerothermodynamics Measurements Laboratory using a uniform heat flux lamp, as described by Kidd and Adams.[23] The time response of the gages was found to be about 0.01 sec. Given BAM6QT run times of about 5.5 to 10.0 seconds, transient measurement effects were considered negligible in post-processing. Two DPO7054 Tektronix oscilloscopes were used to sample data from the heat transfer gages at 100 kHz, with on-the-fly averaging in Hi-Res mode. Data were filtered in post-processing to remove 60 Hz oscillations due to electrical noise. A Kulite model XTEL-190-200A pressure transducer was used to determine the stagnation pressure in the tunnel contraction.

Data were compared to a Fay-Riddell stagnation-point heat-transfer computation. This calculation was based on Anderson's compressible similarity solution for a non-reacting gas at the stagnation point of a sphere and the related empirical correlation obtained by Fay and Riddell.[24] Mach number was assumed constant throughout the run and wall temperature data were taken from the output of the surface thermocouple on the Schmidt-Boelter thermopile.

It is important to note the differences between quiet and noisy flow, aside from noise levels, that can affect heat transfer measurements and calculations. Run time under quiet flow is usually several seconds shorter than that of a noisy run, typically lasting about 5.5 to 6.0 seconds under quiet flow and nearly 10 seconds under noisy flow. The difference is mainly due to a 35% increase in mass flux in quiet runs caused by the bleed suction. Additionally, Mach number is about 5.7 under noisy flow and 6.0 under quiet flow. The Mach number for the BAM6QT under noisy flow is usually stated to be 5.8.[25] This is usually accurate; however, pitot measurements have found Mach numbers near 5.7 at positions farther downstream, presumably due to growth of the nozzle-wall boundary layer.

C. Results and Discussion

Figures 22(a) and (b) show the resulting stagnation point heat transfer rates for two runs conducted under quiet and noisy flow conditions at an initial stagnation pressure of 90 psia. The data set is curtailed to remove startup and shutdown heating. The data indicate that heating under noisy flow is 5% to 25% larger than under quiet flow throughout the run. These differences can be accounted for by the change in Mach number from noisy to quiet flow, and by the difference in mass flux causing unit Reynolds number changes between noisy and quiet runs at the same initial stagnation pressure. Taking these differences into account in the Fay-Riddell calculations, the data from the Schmidt-Boelter transducer agree well with theory. Figure 22(c) shows a maximum deviation of about 7% between experiment and theory. To improve estimates of stagnation temperature and Mach number, cold-wire and pitot-probe data will be obtained.

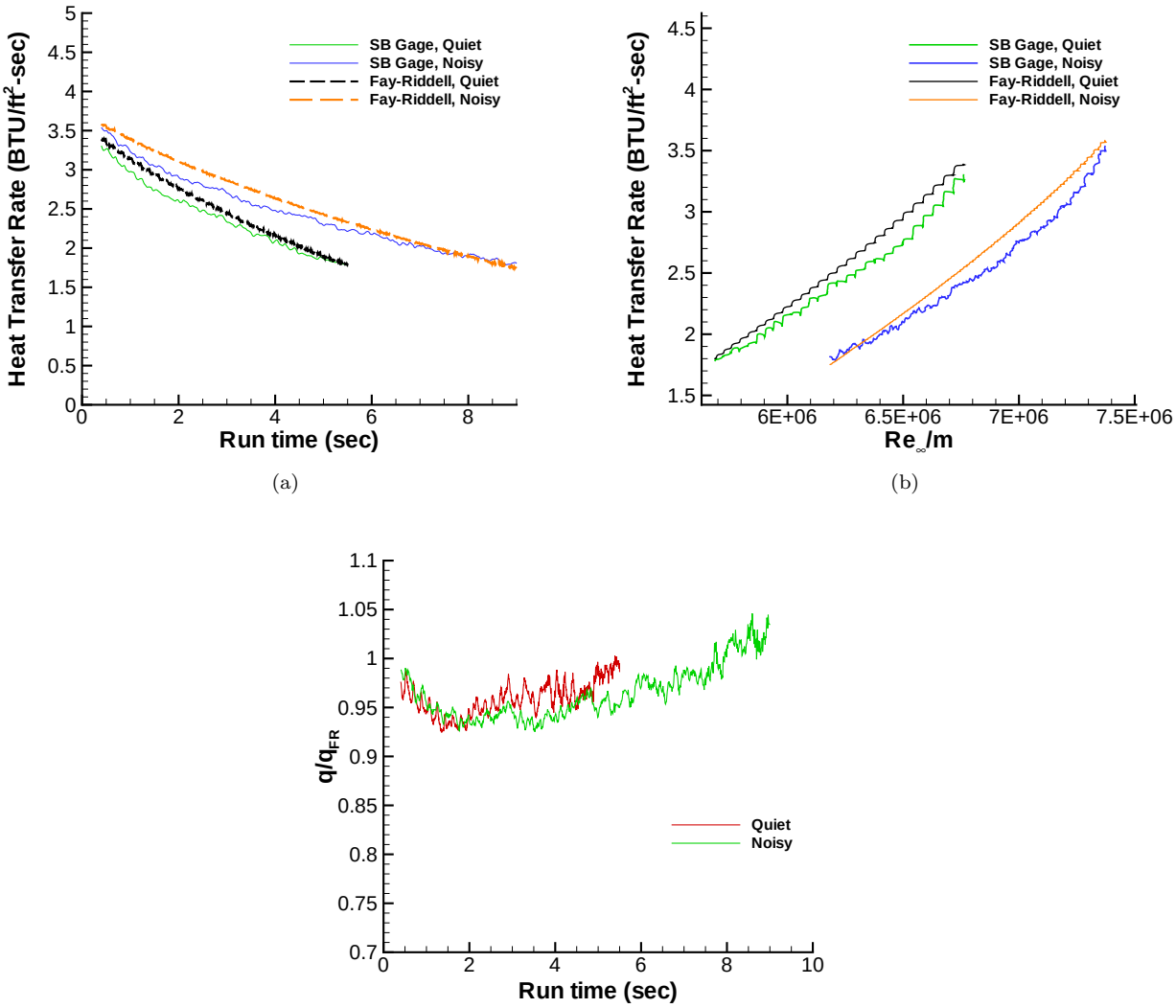

Figure 22: Heat transfer rate at hemisphere stagnation point for $p_{0,i} = 90$ psia, quiet and noisy, with corresponding Fay-Riddell stagnation point heating computations for a sphere. (a) Heating variation with run time, (b) heating variation with freestream Reynolds number, (c) ratio of experimental data to Fay-Riddell computations.

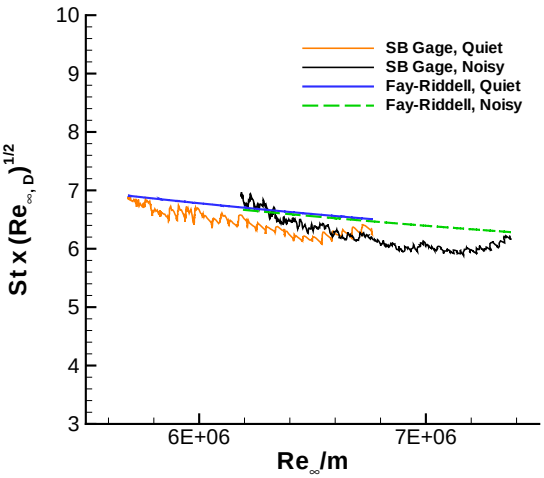

Figure 23: Nondimensional heat transfer parameter, $\mathrm{St} \times (\mathrm{Re}_{\infty,D})^{1/2}$, variation with freestream Reynolds number.

A common method of comparing heat transfer data is to non-dimensionalize using the Stanton number.[24] In this laminar-flow case, the Stanton number multiplied by the square root of the freestream Reynolds number is used to remove Reynolds number dependency. The Stanton number is given by

$$\mathrm{St} \times (\mathrm{Re}_{\infty,D})^{1/2} = \frac{q}{\rho_\infty U_\infty (H_0 - H_w)} \left(\frac{\rho_\infty U_\infty D}{\mu_\infty} \right)^{1/2}$$

where $\mathrm{Re}_{\infty,D}$ is the freestream Reynolds number based on hemisphere diameter, q is the heat transfer rate, H_0 is the total enthalpy, and H_w is the enthalpy at the wall.

Figure 23 gives the resulting comparison between the quiet and noisy cases. The Fay-Riddell calculations for the two cases line up almost exactly, with a small discrepancy likely due to the assumption of constant Mach number throughout the run. Looking at the quiet and noisy heat transfer data, there appears to be a similar pattern to the scatter of data below the Fay-Riddell calculations. Within the accuracy of the present measurements, no effect of tunnel noise can be clearly detected.

D. Future Work

Efforts are proceeding to improve the accuracy of stagnation-point heat-transfer measurements in the BAM6QT. Experiments are being conducted to better determine Mach number and stagnation temperature to improve the accuracy of the calculations. A model of the CEV heatshield is being manufactured to perform experiments similar to Hollis et al.[22] To improve the resolution of measurements of any potential heating effect, five 0.79 mm (1/32 in.)-diameter thermocouples will be positioned near the stagnation point of the model instead of just a single 3.18 mm (1/8 in.)-diameter Schmidt-Boelter gage.

VII. Conclusion

The current maximum quiet pressure of the BAM6QT is about 146 psia, which is the highest pressure at which there is a continuous second of quiet flow. However, useful periods of quiet flow (those with a duration of at least 0.1 seconds) can still be obtained at pressures as high as 169 psia. This range of pressures between 146 and 169 psia is classified as intermittently quiet flow.

A 3-m circular arc compression cone was run with a nearly sharp nosetip (initial radius of 0.16 mm). Second-mode wave growth was detected by PCB 132A31 pressure transducers under quiet flow at high pressures, and for all pressures under noisy flow. What may be transition under quiet flow appears near $N = 15$–19. Transition under quiet flow appears to involve hot-streaks which appear, disappear, and reappear at the aft end of the cone. These hot streaks are not observed under noisy flow. Pitot-probe measurements

of the freestream noise near the back of the cone need to be performed to confirm that the entire model is under quiet flow for the pressures at which the hot streaks were observed. Transition occurs near $N = 9$ under noisy flow. It is unknown why transition occurs at such high N factors on this model.

A 7° half-angle cone with a sharp nosetip was tested with a rough temperature-sensitive paint finish and two smooth finishes. At freestream unit Reynolds numbers of 11×10^6/m, 9×10^6/m, and 8×10^6/m the rough paint finish and the second smooth paint finish showed that tunnel noise had a substantial effect on the crossflow vortices, inducing transition under noisy flow. The first smooth paint finish only showed conclusive evidence of a tunnel noise effect at a Reynolds number of 11×10^6/m. The nature of the effect of distributed roughness on the breakdown of the crossflow vortices is unclear. Roughness height seems to have an effect, as seen when the first smooth paint finish is compared to the rough paint finish. However, there are only negligible differences between the second smooth paint finish and the rough paint finish. The spatial distribution of the roughness is almost certainly important.

Heat-transfer measurements were made at the stagnation point of a hemisphere in an effort to characterize the effect of tunnel noise on heating rates. No effect was found, within the accuracy and resolution of the present measurements.

Acknowledgments

This research was funded by AFOSR under grants FA9550-09-1-0191 and FA9550-08-1-0290, and by the NASA CUIP program. AEDC provided the hemisphere model for the heat transfer measurements.

References

[1]Alba, C., Johnson, H., Bartkowicz, M., Candler, G., and Berger, K., "Boundary Layer Stability Calculations for the HIFiRE-1 Transition Experiment," *Journal of Spacecraft and Rockets*, Vol. 45, No. 6, January 2008, pp. 1125–1133.

[2]Schneider, S. P., "Hypersonic Laminar-Turbulent Transition on Circular Cones and Scramjet Forebodies," *Progress in Aerospace Sciences*, Vol. 40(1-2), February 2004, pp. 1–50.

[3]Beckwith, I. and III, C. M., "Aerothermodynamics and Transition in High-Speed Wind Tunnels at NASA Langley," *Annual Review of Fluid Mechanics*, Vol. 22, 1990, pp. 419–439.

[4]Schneider, S. P., "Effects of High-Speed Tunnel Noise on Laminar-Turbulent Transition," *Journal of Spacecraft and Rockets*, Vol. 38(3), May-June 2001, pp. 323–333.

[5]Schneider, S. P., "Flight Data for Boundary-Layer Transition at Hypersonic and Supersonic Speeds," *Journal of Spacecraft and Rockets*, Vol. 36(1), January-February 1999, pp. 8–20.

[6]Chen, F.-J., Malik, M., and Beckwith, I., "Boundary-Layer Transition on a Cone and Flat Plate at Mach 3.5," *AIAA Journal*, Vol. 27(6), June 1989, pp. 687–693.

[7]Juliano, T. J., Schneider, S. P., Aradag, S., and Knight, D., "Quiet-Flow Ludwieg Tube for Hypersonic Transition Research," *AIAA Journal*, Vol. 46(7), July 2008, pp. 1757–1763.

[8]Wheaton, B. M., Juliano, T. J., Berridge, D. C., Chou, A., Gilbert, P. L., Casper, K. M., Steen, L. E., Schneider, S. P., and Johnson, H. B., "Instability and Transition Measurements in the Mach-6 Quiet Tunnel," *39th AIAA Fluid Dynamics Conference*, June 2009, AIAA-2009-3559.

[9]Schneider, S. P. and Juliano, T. J., "Laminar-Turbulent Transition Measurements in the Boeing/AFOSR Mach-6 Quiet Tunnel," *37th AIAA Fluid Dynamics Conference and Exhibit*, June 2007, AIAA-2007-4489.

[10]Juliano, T. J., Segura, R., Borg, M. P., Casper, K., Michael J. Hannon, J., Wheaton, B. M., and Schneider, S. P., "Starting Issues and Forward-Facing Cavity Resonance in a Hypersonic Quiet Tunnel," *38th Fluid Dynamics Conference and Exhibit*, June 2008, AIAA-2008-3735.

[11]Schneider, S. P. and Haven, C. E., "Quiet-Flow Ludweig Tube for High-Speed Transition Research," *AIAA Journal*, Vol. 33, No. 4, April 1995, pp. 688–693.

[12]Blanchard, A. E., *An Experimental Investigation of Wall-Cooling Effects on Hypersonic Boundary-Layer Stability in a Quiet Wind Tunnel*, Ph.D. thesis, Old Dominion University, 1995.

[13]Balakumar, P. and Kegerise, M. A., "Receptivity of Hypersonic Boundary Layers over Straight and Flared Cones," *48th AIAA Aerospace Sciences Meeting*, January 2010, AIAA-2010-1065.

[14]Johnson, H. B. and Candler, G. V., "Analysis of Laminar-Turbulent Transition in Hypersonic Flight Using PSE-Chem," *36th AIAA Fluid Dynamics Conference and Exhibit*, June 2006, AIAA-2006-3057.

[15]Casper, K. M., *Hypersonic Wind-Tunnel Measurements of Boundary-Layer Pressure Fluctuations*, Master's thesis, Purdue University, July 2009.

[16]Casper, K., Wheaton, B., Johnson, H., and Schneider, S., "Effect of Freestream Noise on Roughness-Induced Transition at Mach 6," *38th Fluid Dynamics Conference and Exhibit*, June 2008, AIAA-2008-4291.

[17]Mack, L., "Stability of Axisymmetric Boundary Layers on Sharp Cones at Hypersonic Mach Numbers," *AIAA 19th Fluid Dynamics, Plasma Dynamics and Lasers Conference*, June 1987, AIAA-87-1413.

[18]Swanson, E. O., *Boundary-Layer Transition on Cones at Angle of Attack in a Mach-6 Quiet Tunnel*, Ph.D. thesis, Purdue University, West Lafayette, Indiana, 2008.

[19]Holden, M., Gustafson, C., Duryea, G., and Hudack, L., "An Experimental Study of Particle-Induced Convective Heating Augmentation," AIAA-1976-320, July 1976.

[20]Hoshizaki, H., Chou, Y., Kulgein, N., and Meyer, J., "Critical Review of Stagnation Point Heat Transfer Theory," Tech. Rep. AFFDL-TR-75-85, Lockheed Palo Alto Research Laboratory, July 1975.

[21]Hollis, B. R., Liechty, D. S., and Wright, M. J., "Transition Onset and Turbulent Heating Measurements for the Mars Science Laboratory Entry Vehicle," *43rd AIAA Aerospace Sciences Meeting and Exhibit*, January 2005, AIAA-2005-1437.

[22]Hollis, B. R., Berger, K. T., and Horvath, T. J., "Aeroheating Testing and Predictions for Project Orion CEV at Turbulent Conditions," *46th AIAA Aerospace Sciences Meeting and Exhibit*, January 2008, AIAA-2008-1226.

[23]Kidd, C. T. and Adams, J. C., "Development of a Heat-Flux Sensor for Commonality of Measurement in AEDC Hypersonic Wind Tunnels," AIAA-2000-2514, June 2000.

[24]Anderson, J. D., *Hypersonic and High-Temperature Gas Dynamics*, American Institute of Aeronautics and Astronautics, Inc., Virginia, 2nd ed., 2006.

[25]Schneider, S. P., Matsumura, S., Rufer, S., Skoch, C., and Swanson, E., "Progress in the Operation of the Boeing/AFOSR Mach-6 Quiet Tunnel," AIAA-2002-3033, June 2002.